

CONFIDENCE SETS FOR PHYLOGENETIC TREES

BY AMY WILLIS

Cornell University

Inferring evolutionary histories (phylogenetic trees) has important applications in biology, criminology and public health. However, phylogenetic trees are complex mathematical objects that reside in a non-Euclidean space, which complicates their analysis. While our mathematical, algorithmic, and probabilistic understanding of the behavior of phylogenies in their metric space is relatively mature, rigorous inferential infrastructure is as yet undeveloped. In this manuscript we unify recent computational and probabilistic advancements to propose a method for constructing tree-valued confidence sets. The procedure accounts for both centre and multiple directions of tree-valued variability, proposing advantages over existing methods that are exploratory and only address a single direction of variability. We demonstrate fast identification of splits with weak and strong support, eliminating problems of simultaneous inference that arise when only bootstrap cladal support is considered. We draw on statistical concepts of block replicates for improved testing, investigating the hypothesis of isotropy in a turtle evolution dataset, identifying the best supported most recent ancestor of the Zika virus (Pacific strains, contrary to media releases in Latin America), and formally test the hypothesis that a Floridian dentist with AIDS infected two of his patients with HIV. The method illustrates connections between variability in Euclidean and tree space, opening phylogenetic tree analysis to techniques available in the multivariate Euclidean setting.

1. Introduction. Evolutionary histories are key data objects in biology, biogeography, criminology, anthropology and immunology. In addition to illuminating interesting ancestral connections, their careful analysis has aided in freeing the innocent [31], reducing accidental disease transmission by healthcare providers [22], and identifying perpetrators of wilful HIV infection [12].

The development of models for inferring evolutionary histories, or *phylogenies*, has become highly sophisticated since its genesis in 1964 [7, 8]. Different models may account for such varied biological possibilities as stochastic coalescence [11], gene duplication [25], and hybridization [9]. However, it may

MSC 2010 subject classifications: Primary 62F03, 62C99; secondary 62H86

Keywords and phrases: phylogenetics, statistical inference, simultaneous testing, non-Euclidean phylogenetics

not be the case that there is a single evolutionary history unanimously implied by all genetic loci, and different genetic sites may conflict with respect to the implied phylogeny [27]. Between the 1960's and the early 2000's this line of research focused on *consensus* methods, which unify collections of evolutionary histories into a single tree. However, more recently, the statistical perspective that observed variability between collections of trees is interesting of itself has gained traction. This has spawned a number of modern methods that utilize the elegant mathematics of tree space to permit new data analysis methods and associated new insights in a number of different contexts [4, 20, 39].

Despite great gains made with respect to exploring (a) the center of a collection of trees [4], and (b) the direction of their variability [20, 21], the literature lacks any statistical method that simultaneously considers both these issues. Additionally, because tree space is not equipped with an inner product, methods for variance exploration have so far only captured a single direction of variability. Furthermore, the geometry of tree boundaries complicates assignment of parametric distributions on the metric space of phylogenetic trees. The approach presented in this paper addresses all of these issues, quantifying multiple directions of variability along with centre, proposing a normal distribution analogue for tree space, and offering a new perspective on embeddings and the relationship between tree space and \mathbb{R}^n .

We begin with an overview of existing mathematical infrastructure, including tree space, manifolds and homeomorphisms, and central limit theorems (Section 2), before developing the necessary statistical infrastructure (Section 3). We describe our confidence set construction procedure in detail (Section 4) and investigate coverage (Section 5), then demonstrate its utility for detecting splits of weak and strong support and in tree-valued hypothesis testing (Section 6). Among our examples we investigate the biogeography of the Zika virus as well as a forensics investigation. A discussion of experimental design for phylogenetics and other questions raised by this method, as well as the relationship between statistics on tree space and Euclidean space, concludes the paper (Sections 7 and 8).

2. Infrastructure. The key innovation of this paper is the construction of confidence sets for phylogenetic tree-valued parameters. We progress the major *probabilistic* advances presented by [1] into a complete statistical framework for inference. To do this we rely on a number of mathematical constructions, including tree space, Fréchet means, and the tree-log-map. While this section is not intended to be self-contained, and we refer the reader to the references for more details, we briefly review some necessary

concepts and introduce notation and a new concept of tree set measurability.

2.1. Tree space. The metric space of phylogenetic trees (\mathcal{T}_m, γ) , or *tree space*, is a complete separable metric space [3, 6, 30] that permits comparison between phylogenetic trees with the same leaf set of cardinality m . The distance $\gamma(T_i, T_j)$ between two trees T_i and T_j accounts for differences with respect to both their tree topologies (branching structure) and branch lengths. The space is constructed by representing each of the $(2m - 3)!!$ possible tree topologies by a single non-negative Euclidean orthant of dimension $m - 3$ (the largest possible number of internal branches). The orthants are then “glued together” along appropriate axes. Specifically, nearest neighbor interchange (NNI) topologies lie in adjacent non-negative orthants along the boundary corresponding to the collapse of the relevant NNI edge. Construction of the space is due to [6].¹

The space is *nonpositively curved* [6], which has resulted in efficient algorithms for calculating geodesic paths [23], means [2, 17] and principal paths [21]. Furthermore, non-positive curvature (NPC) of the space results in unique *Fréchet means*: for a collection of trees $T_1, \dots, T_n \in \mathcal{T}_m$, the sample Fréchet mean

$$\hat{T}_n = \hat{T}_n(T_1, \dots, T_n) := \arg \min_{t \in \mathcal{T}_m} \sum_{i=1}^n \gamma(T_i, t)^2$$

is guaranteed to be unique [2]. This property is an important consideration in investigation of statistics on the space: ensuring identifiability of the target of inference is key to the success of many statistical procedures [35, 26].

2.2. Probability triples. Given guarantees of tree mean uniqueness, we turn our attention to their inference. To maintain rigor, a number of generalizations need to be specified. The use of a underlying probability triple was implicit in [1], though as we look to infer parameters of tree-valued distributions we need to be more explicit.

We begin by constructing a σ -algebra on \mathcal{T}_m . Because \mathcal{T}_m is a metric space we have a well-defined concept of open balls, and thus can generate the Borel algebra by their countable unions, intersections and relative compliments. By construction this a σ -algebra.

¹For generality we consider trees to be unrooted, though by designating a particular leaf as the root the restriction to rooted trees is trivial. Note that [1] considered rooted trees with m leaves; this difference accounts for our use of \mathcal{T}_{m+3} and \mathbb{R}^m in contrast to their use of \mathcal{T}_{m+2} and \mathbb{R}^m .

With our σ -algebra we can now define a measure on this algebra by writing any set in \mathcal{T}_m in the form $A = A_0 \cup \left(\bigcup_{i=1}^{(2m-3)!!} A_i \right)$ for $A_i, i \geq 1$, a collection of trees wholly contained within an i -th enumeration of the topologies, and A_0 the collection of trees in A with one or more internal vertices of degree 4 or less (equivalently, trees on the orthant boundaries of \mathcal{T}_m). We then define $\mu(A) = \sum_{i \geq 1} \mu_B(A_i)$ for μ_B the Euclidean Borel measure of dimension $m-3$. This preserves σ -additivity because the Borel measure of any orthant boundary is zero, and there are only finitely many such boundaries. While this construction would be sufficient for most purposes, it is not a complete measure space. However, its completion may be trivially defined in the usual way (by appending all sets of Borel measure zero) to give an analogue of Lebesgue-measurable sets in \mathcal{T}_m , which we call $\mathcal{L}(\mathcal{T}_m)$. The latter construction will be implicitly used as our σ -algebra henceforth, and we have a preliminary complete measure space $(\Omega, \mathcal{L}(\mathcal{T}_m), \mu)$. Finally, for a probability measure $F : \mathcal{L}(\mathcal{T}_m) \rightarrow [0, 1]$, defined with respect to the volume measure μ , we obtain a probability triple $(\Omega, \mathcal{L}(\mathcal{T}_m), F)$.

2.3. Limit theorems and the log map. While theory for central limit theorems for Fréchet means on metric spaces has been well-developed [5], these generally rely on homeomorphisms to \mathbb{R}^n from measureable subsets of the space known to contain the true Fréchet mean μ of the probability measure F ,

$$\mu = \arg \min_{u \in \mathcal{T}_m} \int \gamma(q, u)^2 F(dq).$$

However, due to the orthant multiplicities of our metric space of interest, \mathcal{T}_m , inverse functions will not exist for candidate homeomorphisms except restricted to subsets wholly contained in a single orthant, because tree space cannot be completely embedded in Euclidean space (see, for example, [20, p. 2720]). Thus without assuming the topology of the true mean *a priori*, general results for CLTs on manifolds are insufficient for tree mean inference.

To overcome these difficulties, [1] developed a mapping from \mathcal{T}_{m+3} to \mathbb{R}^m and proved mapped multivariate normality of the sample Fréchet mean around the true Fréchet mean, deriving expressions for the covariance based on the distribution F . While the proposed mapping, called the log map, is not a homeomorphism, it elegantly deals with samples from multiple topologies, taking advantage of similarities between tree space and Euclidean space while respecting their different combinatorial structures.

The log map function of [1], $\log_{T^*}(T)$, captures both the distance and direction from a base tree T^* to a target tree T . For now, we consider only base trees off the orthant boundaries, though we return to this issue in

Section 7. Formally, $\log_{T^*}(T) : \mathcal{T}_{m+3} \rightarrow \mathbb{R}^m$ is defined as

$$\log_{T^*}(T) = \gamma(T^*, T) \mathbf{v}_{T^*}(T),$$

where $\gamma(T^*, T)$ is the geodesic distance between T^* and T , and $\mathbf{v}_{T^*}(T)$ is a specifically chosen unit vector from T^* to T that reflects the direction of the first segment of the geodesic (details below). The modified log map (MLM) positions this vector to originate from the base tree,

$$\Phi_{T^*}(T) = \log_{T^*}(T) + \mathbf{t}^*,$$

for \mathbf{t}^* the coordinates in \mathbb{R}^m of T^* 's edge lengths. For a meticulous description of the correct permutations of the ordering of the edge lengths necessary to maintain invariance across multiple argument topologies, see [1].

The intuition behind $\mathbf{v}_{T^*}(T)$ can best be illustrated via the MLM, and may be seen in Figure 1. For a target tree in the same orthant as the base tree (identical topologies), the MLM coincides with a Euclidean representation of the target tree, that is, is an m -vector with all positive components reflecting the lengths of the target tree's internal branches. For a target tree in an adjacent orthant (nearest neighbor interchange topology), the MLM vector has a single negative component with magnitude equal to the length of the branch present on the target tree but not present on the base tree, with the remaining components positive (adjusted to reflect the branch lengths of the target tree). If the target tree is more topologically distinct than a NNI interchange from the base tree, the simplest visualization is to follow the initial segment of the geodesic path (the segment contained in the same orthant as the base tree) for the length of the geodesic across (potentially more than one) Euclidean orthant boundaries. To employ the notation of [23], this is equivalent to finding any tree of fraction λ along the geodesic, for

$$0 < \lambda < \frac{\|A_1\|}{\|A_1\| + \|B_1\|}$$

(obtained by solving Theorem 2.4 of [23] for $i = 0$), representing this tree as a Euclidean vector \mathbf{s}^* with all positive coordinates and the same edge ordering as \mathbf{t}^* , then calculating the log map as

$$\Phi_{T^*}(T) = \mathbf{t}^* + \frac{\mathbf{s}^* - \mathbf{t}^*}{\|\mathbf{s}^* - \mathbf{t}^*\|} d(T^*, T).$$

Note that A_1 and B_1 above refer to the first elements of the partitions of the geodesic support of the geodesic path between T^* and T (as in [23]). The particular choice of λ does not affect $\Phi_{T^*}(T)$ because $\frac{\mathbf{s}^* - \mathbf{t}^*}{\|\mathbf{s}^* - \mathbf{t}^*\|}$ is a unit vector. Henceforth we will refer to the MLM as the log map for convenience.

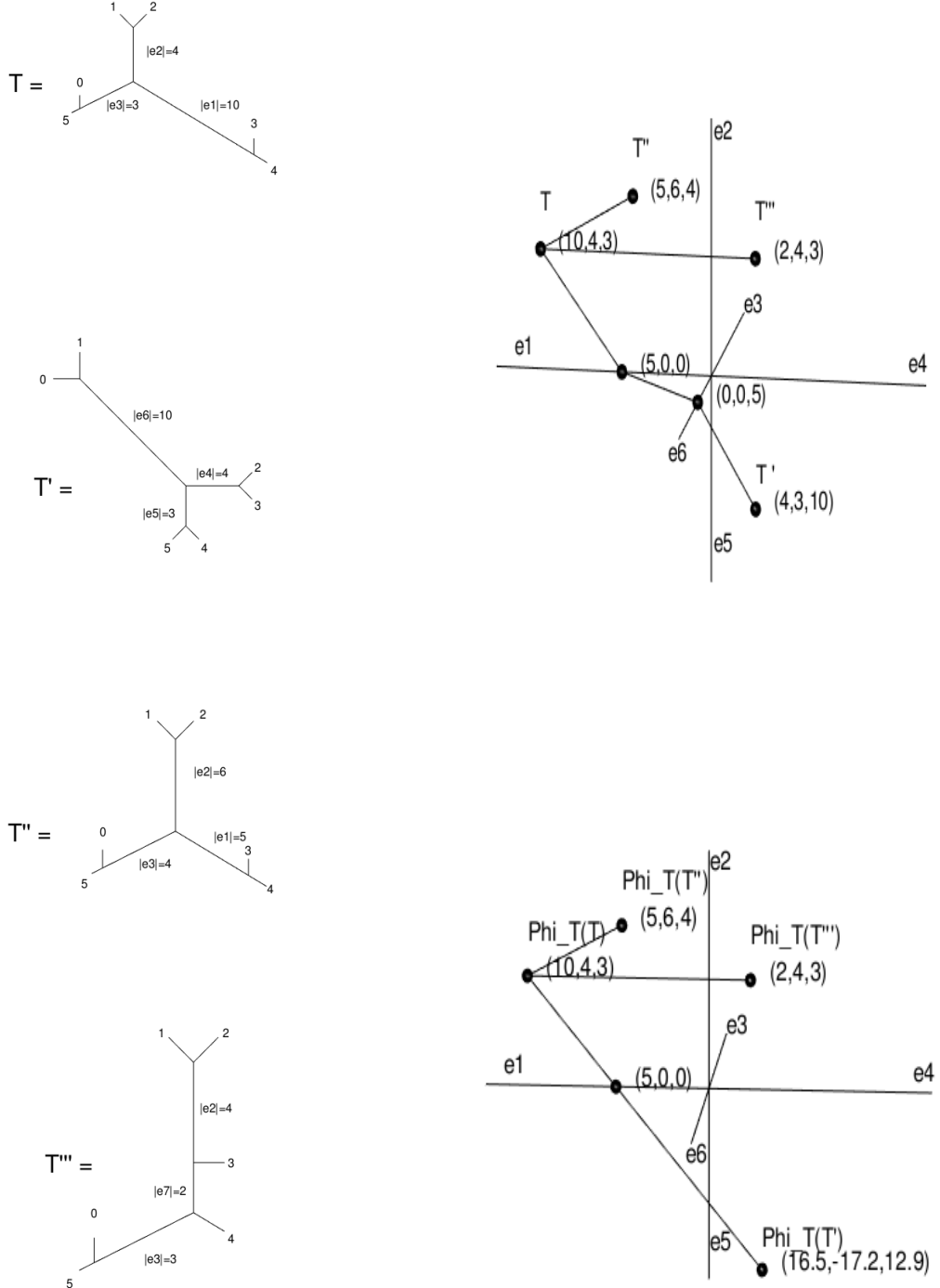


FIG 1. Four phylogenetic trees (left panel), a representation of tree space (top right), and its embedding in Euclidean space via the log map (bottom right). The geodesic path between tree T illustrates how geodesics “bend” across the orthant (topology) boundaries. By comparison, the log map does not bend, but captures the length and direction of the geodesic by extending the first linear segment of the path.

3. Statistical infrastructure. Many modern investigations in phylogenetics give rise to tree-valued information, where each of several sources or combinations of data suggest their own, possibly conflicting evolutionary histories. Thus, as the primary data objects for our method, consider n unrooted trees sampled on the same collection of $m + 3$ taxa, $m \geq 1$. Thus we have $T_1, T_2, \dots, T_n \in \mathcal{T}_{m+3}$ as our “observations”. We return to a discussion of potential sources of trees as data objects in Sections 7.3.

We consider these observations to be observed *iid* from some unknown distribution on \mathcal{T}_{m+3} , call it F , which represents the variability in this set of trees (which, if desired, could be built up through a stochastic model for nucleic acid base substitutions or a population dynamics model). Suppose that F has a finite Fréchet function $G(u) = \int_{\mathcal{T}_{m+3}} \gamma(q, u)^2 F(dq)$, and Fréchet mean $T^* = \arg \min_{u \in \mathcal{T}_{m+3}} G(u)$ in a top-dimensional stratum. Using the notation defined in Section 2, we state our key theorem.

THEOREM 3.1. *Suppose F satisfies $F(D) = 0$, where D is the set of trees with at least one internal branch of length zero. Then, for the sample Fréchet mean \hat{T}_n , as n becomes large,*

$$\Phi_{\hat{T}_n}(\hat{T}_n) \rightarrow \mathcal{N}\left(\Phi_{T^*}(T^*), \frac{\Sigma}{n}\right),$$

for Σ a covariance matrix determined by the structure of F .

PROOF. The result follows from [1, Theorem 2] after noting that our regularity condition on the orthant boundaries is T^* -independent, since $\mathcal{D}_{T^*} \subset D$ for all T^* , where \mathcal{D}_{T^*} is as defined in [1, Definition 1]. Thus the measure of the boundaries of the maximal cells of the subdivisions are necessarily F -null for distributions that satisfy our condition for any Fréchet mean. We note that this considers the variability attributable to inferring both the log map’s argument T^* and the log map $\Phi_{T^*}(\cdot)$ itself. \square

This theorem forms the foundation of our tree inference procedure. However, it raises a number of important issues regarding estimation that must be resolved to bridge the gap between the existing probability theory and the (hitherto undeveloped) statistics. We address these in turn below.

3.1. Mean tree. Given Theorem 3.1, a natural candidate for estimating T^* is \hat{T}_n . Furthermore, [41, Theorem p. 592] guarantees strong \mathcal{T}_{m+3} -consistency of the (unique) sample Fréchet mean under weaker conditions than [1, Theorem 2] and Theorem 3.1. Efficient algorithms for sample Fréchet

mean computation lend an additional appealing quality [2, 17], as do the results of [4].

As statistical inference for tree space develops, estimators of T^* other than \hat{T}_n are likely to be developed, supported by their own CLTs and LLNs. The procedure described in Section 4 would be unchanged if the practitioner were to use a different normally distributed true Fréchet mean estimate.

3.2. Log-map function. Masked by notation is the need to estimate $\Phi_{T^*}(\cdot)$, the log-map function. This function is fully determined by its base tree T^* , which must be estimated. The above discussion regarding tree mean estimation points to estimating the function $\log_{T^*}(\cdot)$ by $\log_{\hat{T}_n}(\cdot)$, however functional consistency needs to be verified. Since \mathcal{T}_{m+3} is not Hilbert, and the function under question is not linear, we do not know of any results that immediately guarantee this.

PROPOSITION 1. *Consider trees $T_1, \dots, T_n \in \mathcal{T}_m$ drawn from some distribution F on \mathcal{T}_{m+3} with true Fréchet mean T^* , not located on an orthant boundary, that satisfies*

$$(3.1) \quad \int_{\mathcal{T}_{m+3}} \gamma(\mathbf{0}_{\mathcal{T}_{m+3}}, T)^2 dF(T) < \infty.$$

For a fixed tree $t \in \mathcal{T}_{m+3}$, consider the function $\log_{(\cdot)}(t) : \mathcal{T}_{m+3} \rightarrow \mathbb{R}^m$. Then for all $t \in \mathcal{T}_{m+3}$ we have that $\Phi_{\hat{T}_n}(t)$ converges almost surely to $\Phi_{T^}(t)$ in \mathbb{R}^m as $n \rightarrow \infty$.*

PROOF. Almost sure convergence is preserved by addition and multiplication, thus it is sufficient to show that (a) $\hat{\mathbf{t}}_n^* \xrightarrow{a.s.} \mathbf{t}^*$ in \mathbb{R}^m , (b) $\gamma(\hat{T}_n, t) \xrightarrow{a.s.} \gamma(T^*, t)$ in \mathbb{R} , and (c) $\mathbf{v}_{\hat{T}_n}(t) \xrightarrow{a.s.} \mathbf{v}_{T^*}(t)$ in \mathbb{R} for all t . From [41], combined with Condition 3.1, we have that $\hat{T}_n \xrightarrow{a.s.} T^*$ in \mathcal{T}_{m+3} . Hence for $n > m$ for some m , we are guaranteed that the sample mean will be in the same orthant as the true mean and thus for $n > m$, $|\hat{\mathbf{t}}_n^* - \mathbf{t}^*| = \gamma(\hat{T}_n, T^*) \xrightarrow{a.s.} 0$, hence (a). $\gamma(\cdot, \cdot)$ is a bicontinuous function (metrics are guaranteed this property), and thus the continuous mapping theorem guarantees (b). For (c), we claim $\mathbf{v}_{(\cdot)}(t)$ is a continuous function. We need only consider possible discontinuities in the carrying orthant sequence ($\gamma(\cdot, \cdot)$ may be bicontinuous but this is no guarantee that the path will be). However, this follows from construction [1, Paragraph 1, p12], and in particular, the existence of log map directional derivatives and [1, Theorem 2]. \square

Thus we estimate the true log map function with the sample log map function.

3.3. Covariance estimation. Perhaps the most substantial complication when transitioning from Theorem 3.1 to a statistical inference procedure is the estimation of covariance matrix Σ . While this matrix can (theoretically) be calculated given known F , we wish to avoid strong assumptions on F , and in particular, we wish to avoid *structural* assumptions. Furthermore, calculating this matrix in practice would require integration across multiple orthants, and despite the advances in tree integration by [38], this will generally be intractable for distributions with full support on the space.

The approach we present here takes advantage of the intrinsic connection between tree space and Euclidean space. Consider our estimate of the log map, $\Phi_{\hat{T}_n}(\cdot)$, and consider the collection of \mathbb{R}^m -valued objects $\Phi_{\hat{T}_n}(T_1), \Phi_{\hat{T}_n}(T_2), \dots, \Phi_{\hat{T}_n}(T_n)$, which we know has (sample) mean $\Phi_{\hat{T}_n}(\hat{T}_n)$ [1, Lemma 3, setting $\mu(T) = \mathbb{1}_{\{T \in \{T_i\}\}}(T)$ and the base tree as \hat{T}_n]. The construction of the log map tells us that for trees in the same orthant as \hat{T}_n , this mapping gives us the natural embedding of the trees in the same Euclidean orthant as \hat{T}_n . However, for trees with distinct topologies, the log map projects to an \mathbb{R}^m orthant given by continuing the direction of the initial geodesic segment of the geodesic path between the base and target trees. Thus we have n \mathbb{R}^m -valued observations, generally spanning multiple orthants, forming a point cloud around their mean, with directional variability indicating edges (equivalently, splits) that may be estimated with greatest and least precision.

We propose to use an unstructured covariance estimator to estimate Σ via the implied covariance of $\Phi_{\hat{T}_n}(T_1), \Phi_{\hat{T}_n}(T_2), \dots, \Phi_{\hat{T}_n}(T_n)$. This has the obvious advantage of being independent of the distribution of the individual trees T_1, \dots, T_n , and thus not requiring calculation nor estimation of the moments of F , which are intractable for all acceptably flexible candidate F 's. Thus if a sufficiently large tree sample is available, the classic estimator

$$(3.2) \quad S = \frac{1}{n-1} \sum_{i=1}^n \left(\Phi_{\hat{T}_n}(T_i) - \Phi_{\hat{T}_n}(\hat{T}_n) \right) \left(\Phi_{\hat{T}_n}(T_i) - \Phi_{\hat{T}_n}(\hat{T}_n) \right)^T$$

is unbiased for Σ and has distribution that converges to a rescaled Wishart distribution if the $\Phi_{\hat{T}_n}(T_i)$'s are approximately normally distributed [34]. However, this estimate will be highly unstable when the number of trees is small compared to the number of leaves on the trees. Without wishing to make additional assumptions on covariance structure, stability could be introduced by imposing sparsity on the estimate. In addition to reducing variance, sparse estimates have the advantage of interpretability, because visualizing directions of variability across a large number of directions can be simplified by reducing the number of possible directions. While we obviously

do not want to collapse trees to have a smaller number of edges, this approach may be useful when we wish to determine which splits have the least support. Sparse estimates accompanied by asymptotics (e.g. [14]) lend stability and interpretability to our method of detecting tree valued variability, trading off for bias and a non-standard pivot distribution. Note that our confidence set is constructed via the precision matrix (inverse covariance) and thus we prefer sparsity in the precision rather than covariance matrix.

4. Procedure. Having addressed questions of estimation in Section 3, we now give a complete description of the method for confidence set construction.

1. For trees $T_1, \dots, T_n \in \mathcal{T}_{m+3}$, calculate the mean tree \hat{T}_n using the proximal point algorithm of ([2], Algorithm 4.2; see also [3]).
2. Calculate the Euclidean projections under the sample log map: $\Phi_{\hat{T}_n}(T_1), \Phi_{\hat{T}_n}(T_2), \dots, \Phi_{\hat{T}_n}(T_n)$.
3. Estimate the true tree T^* by \hat{T}_n , and the precision matrix Σ^{-1} by S^{-1} (Eq. 3.2) or with a sparse estimate.
4. Define

$$\overline{\Phi_{\hat{T}_n}(T)} = \frac{1}{n} \sum_{i=1}^n \Phi_{\hat{T}_n}(T_i),$$

an object in \mathbb{R}^m . Construct a $100(1 - \alpha)\%$ confidence hull for T^* , the true Fréchet mean of the data generating distribution, via

$$(4.1) \quad A = \left\{ T_0 \in \mathcal{T}_{m+3} : \right. \\ \left. \left(\overline{\Phi_{\hat{T}_n}(T)} - \Phi_{\hat{T}_n}(T_0) \right)^T S^{-1} \left(\overline{\Phi_{\hat{T}_n}(T)} - \Phi_{\hat{T}_n}(T_0) \right) \right. \\ \left. < \frac{m(n-1)}{n(n-m)} F_{m,n-m}(1 - \alpha) \right\},$$

modifying the pivot distribution or degrees of freedom as appropriate for a different estimator of the precision. The above combines Euclidean multivariate results from [34] with the tree CLT of [1].

5. For a candidate true Fréchet mean tree T_0 , if $T_0 \in A$, conclude that T_0 is contained in the $100(1 - \alpha)\%$ confidence set for the true tree mean T^* .

Due to inherent difficulties with visualizing the space of phylogenetic trees, especially for a large leaf set, it is generally not advisable (*viz.*, computationally) to construct the confidence set in \mathcal{T}_{m+3} . In place of this we advocate

construction under the log map, i.e. $\Phi_{\hat{T}_n}(A)$. Examples of the utility in leaving the set transformed are given Section 6.

Another familiar analysis tool that arises from this procedure is to use S (or $(\hat{\Sigma}^{-1})^{-1}$) to estimate the principal directions of variability in the $\Phi_{\hat{T}_n}(T_1), \dots, \Phi_{\hat{T}_n}(T_n)$ via principal components analysis. The axes of the \mathbb{R}^m ellipsoid indicate the relative directions of precision, and the ellipsoid can be uniformly shrunk (e.g. by shrinking α) to be wholly contained in the same orthant as \hat{T}_n . This gives an unambiguous indication of the relative confidence in the edges of the estimated tree. Note that while the procedure is unambiguous about the trees contained in the confidence set for a given confidence level α , to move from S to higher order principal components a modification is needed, because for any $x \in \mathbb{R}^m$, $\{T \in \mathcal{T}_{m+3} : \Phi_{\hat{T}_n}(T) = x\}$ may contain multiple elements. Thus multiple higher order principal components may need to be searched through to truly ambiguously second, third, and higher directions of greatest variability.

5. Coverage. It is natural to be skeptical of the application of asymptotics to finite sample settings, and for this reason we investigate coverage of the procedure for two different phylogenetic trees and a variety of sample sizes n . The investigation was conducted by first selecting a “true” tree and using this tree to simulate $1000 \times n$ draws of aligned base pairs (350 base pairs for the HIV tree, 500 for the Zika tree) under a simple HKY model using seq-gen [24], then estimating the $1000 \times n$ trees from the aligned base pairs under a HKY model using phyML [10]. These trees were then grouped into 1000 collections of n samples, and for each collection the sample mean was calculated and the confidence set from Eq. 4.1 was constructed for each level α of interest. The proportion of the 1000 confidence sets that contain the true tree gives the estimated coverage of the $100(1 - \alpha)\%$ confidence set.

The results of the simulation study are reported in Table 1. For the tree with 5 leaves, coverage is low, and decreasing with the size of the sample n . However for a tree with 8 leaves the coverage is consistently within 2% of the desired coverage for $\alpha \leq 0.05$, and no more than 5% less than controlled for at $\alpha = 0.1$. Therefore we advise practitioners interested in inferring small trees to construct their confident sets using a smaller level α than the desired coverage in order to actually obtain the desired coverage. For example, with a sample size of 20 trees and a tree target of 5 leaves, constructing the confidence set using $\alpha = 0.01$ would lead to coverage near 95% (Table 1) for a tree with similar characteristics to the HIV tree (see **Software** for access information) and a true tree generating process of HKY. We acknowledge the simplicity of this simulation study, and recommend that if the practitioner

TABLE 1

Estimated coverage of the confidence set procedure. Two different “true” trees from Section 6 were used to generate base pair alignments, and then estimates of the true trees were calculated based on the alignments. These estimates were grouped together into 1000 samples of size n , and the procedure from Section 4 was used to construct the confidence set. The proportion of confidence sets containing the true trees is reported. Exact coverage would be signified by (90, 95, 99, 99.9)%.

| T_0 : True tree | $m + 3$: Leaf count of T_0 | n : Sample size | Coverage (%): $\alpha = (0.10, 0.05, 0.01, 0.001)$ |
|-------------------|-------------------------------|-------------------|--|
| HIV tree | 5 | 20 | (78.1, 87.7, 95.5, 99.4) |
| HIV tree | 5 | 50 | (67.8, 78.3, 91.8, 97.9) |
| HIV tree | 5 | 100 | (56.5, 66.4, 85.2, 93.5) |
| Zika tree | 8 | 20 | (89.0, 93.2, 98.6, 99.3) |
| Zika tree | 8 | 50 | (85.4, 92.3, 97.6, 99.6) |
| Zika tree | 8 | 100 | (87.2, 93.8, 97.9, 99.6) |

could obtain an approximate estimate of the true tree the simulation could be repeated using the model under study and the obtained sample size in order to find a better confidence level for achieving the desired coverage.

It is interesting to note that the coverage decreases with larger sample sizes, at least for smaller trees. We conjecture that this is due to the difference between the multivariate normal distribution and the distribution of HKY-distributed trees under the log map, $\Phi_{T^*}(F_{HKY})$, for T^* the true Fréchet mean of F_{HKY} , the HKY distribution in tree space. This difference becomes increasingly realized as larger samples are drawn from an HKY model. The assumption that these distributions are approximately equal is necessary to obtain Wishart-distributed covariance estimates and thus the correct pivot distribution for the confidence set construction. The contours of F_{HKY} are not known, and nor is their shape in \mathbb{R}^m under the log map, but we believe them to be unlikely to correspond identically with those of a multivariate normal. Thus for a larger sample of trees this approximation is poorer and the pivot distribution is more poorly approximated by an F -distribution, reducing the coverage. Note that we expect the covariance estimate to be improved with larger sample sizes, and for this reason we conjecture that it is the underlying distribution and not the covariance estimate that is affecting coverage. This is further supported by the observation that the coverage is improved for larger trees.

6. Examples. We have claimed utility of the proposed method for fast identification of edges of least support via the covariance estimate, and for tree-valued inference. We proceed to demonstrate that the method works as intended, investigating a turtle phylogeny dataset for which [21] identified to have no axis of greatest (tree-valued) variability, before demonstrating its

strengths with respect to inference on two examples of interest to a general audience. A discussion of tree-independence in these case studies is deferred to Section 7.4.

6.1. *Isotropic turtles.* [33] investigated over-division of the *Pseudemys* (*P.*) genus of North American freshwater turtles, using a dataset of 86 turtles representing 13 taxa, of which 9 taxa represent subdivisions of the genus under question. A single turtle was chosen to represent each taxa and the tree was built based on a single representative of each of the 13 taxa. This process was repeated 100 times to generate 100 trees, with each tree based on a different combination of turtle representatives of the taxa. The authors have kindly provided the 100 trees in \mathcal{T}_{13} (estimated using MrBayes [29]), which we analyze using the procedure described in Section 4.

Considering the components of the $\Phi_{\hat{T}_n}(T_1), \dots, \Phi_{\hat{T}_n}(T_{100})$ along with their estimated standard deviations (square root of the diagonal elements of S) clearly demonstrates 4 branches with strong support and 6 branches with very weak support (distributions centred near 0). Outgroups were introduced by [33] to show relatives that are known to be taxonomically distinct, and 3 of the splits with strong support correspond to splits that separate the outgroups from the *Pseudemys* subgroups. The remaining branch of strong support corresponds to *P. gorzugi*, corresponding identically with [33, Table 3], which identifies this taxa to be most probably taxonomically distinct. All other splits are highly questionable, and we concur with [33] in concluding that the phylogenetic division of *Pseudemys* is oversplit, with far fewer taxa than previously believed.

[21] applied the stochastic principal components geodesic algorithm to this dataset, concluding isotropy due to no distribution around a geodesic of greatest variability. Our inferential framework is ideal for formally testing this hypothesis, because it amounts to testing for sphericity of the covariance matrix of the observations under the sample log map. With this sample size and covariance dimension is unrealistic to think that usual multivariate sphericity tests (e.g. [28]) will be exact, however to refute isotropy only two directions of differential variability need to be found. To exclude issues arising from post-selection inference we use [33, Table 3] to hypothesize that the *P. gorzugi* split will have less variability than the remaining *Pseudemys* splits. Levene tests' p-values for the pairwise comparisons have 5 values between 10^{-8} and 10^{-21} , and one p-value of 0.122. Even with family-wise error rate control, this provides very strong evidence that not all directions of variability are equally variable, and we conclude that the data provides strong evidence against isotropy. It is worth noting that the failure of the

principal geodesic algorithm to find a direction of greatest variability in this dataset does not imply that the data is isotropic in the strict multivariate sense. Multiple directions of similar variability are far more likely to cause non-convergence. We observe slowly decaying eigenvalues of the sample covariance matrix in the turtles dataset, which supports this conclusion and concurs with [21].

6.2. Zika origins. The implications of the Zika virus' spread has caught worldwide attention. The virus is known to have originated in Africa, with media releases in South America purporting that the virus arrived across the Atlantic ocean [18, 19]. We investigate this claim by tracing the biogeography of the current Zika outbreak in South America, concluding strong evidence that the most recent ancestor of the South American outbreak was in fact from the Pacific, whose most recent ancestor was from South-Eastern Asia, and thus that the virus traveled east from Africa, rather than west.

All available complete Zika genome sequences with complete location and year information were obtained from GenBank on June 7, 2016. We categorized the sequences by location and year (Figure 2, left panel), and considered different samples within the same category as block replicates. We then draw one sample from each category, align the sequences, and fit a simple HKY85 model to the phylogeny. We repeat this 150 times to have 150 evolutionary histories reflecting the within-virus variability. Figure 2 (left panel) shows the sample Fréchet mean.

Based on histograms of the log map coordinates' marginal distributions, we notice 3 directions of strong support (always positive coordinates) and 2 directions of uncertain support (some negative coordinates). The edges of strong support can be seen in Figure 2 (right panel), along with the confidence set implied by the procedure outlined in Section 4. We can clearly see that the most recent common ancestor of the South American samples was in the Pacific (horizontal direction), and given the tight clustering centred far from the origin we conclude high confidence in this conclusion. The p-value for the null hypothesis that the true Fréchet mean lacks these branches is less than 10^{-16} . This hypothesis test and our confidence set in Figure 2 accounts and adjusts for the remaining 2 splits.

The claim of most recent ancestry from Pacific-Asia corroborates findings from April of this year [37, 36, 32]. However, we wish to note that these papers claim strong bootstrap support for the order of divergence of the virus within Africa ([32] claims 99% support for African order of divergence; [36] claims 100%) and also the order of Asia-Pacific divergence from Africa ([32] claims 95% support; [36] again claims 100%). However, the marginal distri-

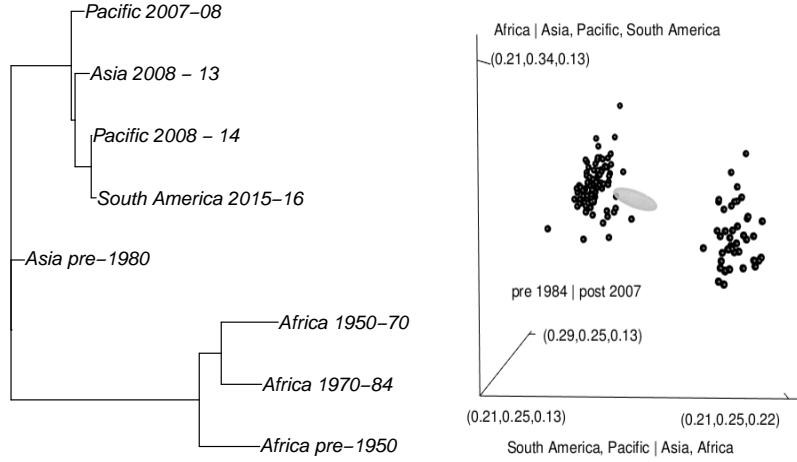


FIG 2. (left) The Fréchet mean of 150 Zika phylogenies obtained by permuting the representative of the collection of patients with similar virus spatiotemporal information. (right) 3 coordinates of the 5-dimensional log maps (with the sample Fréchet mean as the base of the map) of the 150 trees (points), and the 3-dimensional projection of the 95% confidence interval for the true Fréchet mean (ellipsoid). In particular, we have high confidence that the most recent common ancestor of the current South American strain is the Pacific strain (horizontal direction), rather than an African or Asian strain. The 2 clusters are due to the partition of samples built with a particular Asia 2008-13 representative: most samples in this group were pre-2011, while one sample is from 2012. The choice to keep these categories is due to the wish to keep the number of splits small, and the need to obtain enough representatives in each category to accurately and honestly estimate the within-category variance. The merits of this choice are discussed in Section 7.4.

butions of the log map coordinates that reflect these edges suggests some uncertainty after accounting for the within-continent variability. We do not claim that these splits do not exist (a question we leave to tree-model specialists), only that our method gives a more realistic measure of confidence in these edges than bootstrap support percentages. The fast mutation rate of the Zika virus [16] suggests that it is important to account for the variability of the virus even within similar spatiotemporal characteristics, and we argue that failing to account for statistical variability leads to overstated measures of confidence in the phylogenies.

6.3. Dental forensics. In this example we investigate the hypothesis that two HIV-positive patients of a Floridian dentist with AIDS contracted HIV from the dentist. This question was formally investigated by the National

Centre for Infectious Diseases in 1992, culminating in a report concluding transmission to the patients from the dentist [22]. The report considered several different analyses, including the within-patient HIV variation (HIV is known to mutate rapidly), and a phylogenetic analysis. Here we unify these two distinct elements of the report into a single inferential method that accounts for both within- and across-patient variation of the virus.

Amino acid sequences from the V3 region of the HIV virus of the dentist (8 replicates), patient A (6 replicates), patient B (14), a local control (2), and a non-local control (2) were obtained from GenBank. We consider all possible combinations of a dentist sequence, a patient A sequence, a patient B sequence, a local control sequence, and a nonlocal control sequence, to have $8 \times 6 \times 14 \times 2 \times 2 = 2688$ combinations of sequences. For each of these combinations we aligned the sequences using Clustal [15], and estimated the underlying tree using PhyML and a HKY85 model [10]. The mean tree and log maps were then calculated using the procedure detailed in Section 4. We favor a simple model and default parameters, acknowledging potential improvements from more complex models and tuned parameters but noting they are unlikely to substantially affect the results of our investigation.

The projected trees under the sample log map are depicted in Figure 3. We observe approximately equal variance (directional radii of the point cloud) in both branches, however the mean length of the branch separating the dentist and patients from the controls is large relative to its variability. The null that this edge is not present on the true tree is rejected with $p < 10^{-13}$, and thus we conclude with high confidence that the dentist infected the two patients. The remaining branch indicates the relative similarity of the dentist's sequences to those of patient A and patient B (which patient was infected more recently, *viz.*, closer to the date of blood sample collection), and we reject the null hypothesis that there is a leaf more closely related to the dentist than patient A ($p = 0.0009$). It is critical to note the simultaneous accounting for within and across patient similarity in this procedure, and thus it utilizes the information available to the fullest extent and removes the need to separately consider intra/interperson sequence analysis as was necessary in the original investigation [22].

7. Discussion. A number of key considerations are discussed before concluding the manuscript.

7.1. Degeneracy. It is important to note that the asymptotics differ when the true Fréchet mean falls on a strata of codimensions 1 or higher.

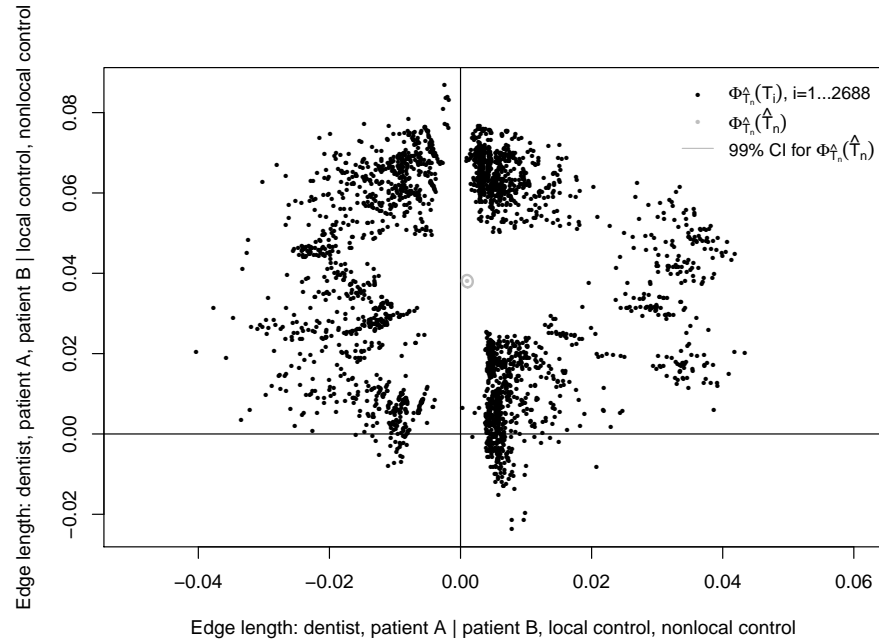


FIG 3. The estimated phylogenies of the HIV viruses of a dentist, two patients of the dentist, a control from the local population, and a control from a distinct population. The different phylogenies were obtained by permuting the representative sequences of each individual. A confidence interval for the true Fréchet mean tree suggests infection of the patients by the dentist, given small variability of this edge length relative to its mean (vertical direction). The remaining branch (horizontal direction) indicates that patient A was infected more recently ($p = 0.0009$). Note that multivariate tree mean asymptotics scale similarly to the univariate case: the major and minor axes of the ellipsoidal confidence set scale with the inverse of the square root of the sample size.

The log map remains multivariate normal on the branches whose means do not correspond to co-faces, with the co-facing branches converging to either a degenerate distribution or a truncated multivariate normal distribution ([1, Theorem 3], [13]). While no statistical tests exist for assessing whether a Fréchet mean lies on a codimension, we did not observe any sample means on strata of co-dimension 1 in our examples. Reduced variability in co-dimension asymptotics lead us to expect faster convergence to the degenerate branches, which we use to justify our use of the usual asymptotics.

Again, while we did not observe this in our examples, in the event that our estimated covariance matrix of the log map is not full rank (at least 1 branch is observed to be perfectly parameterized by a linear combination of other branches) we can restrict our attention to a full rank subset of the branches, using (if inference is desired) that the distribution of the dependent branches is marginally normal (a characterization of the multivariate normal is that all linear combinations are normally distributed). Similarly, if the sample variance of any one branch is zero we adapt the procedure by determining that branch to exist with high probability, and constructing confidence intervals on the subtrees on either side of the zero-variance branch. Note that to maintain $100(1 - \alpha)\%$ coverage globally an adjustment would need to be made marginally to the coverage probability of the individual confidence sets.

7.2. Extension to incorporate tree uncertainty. It is important to note that the trees that we consider as data points will generally be estimated, not known exactly. Thus inherent in each observation is a possibly differing measure of certainty. We conjecture that this could be incorporated into the above procedure using the statistical framework of metaanalysis to account for measurement error, similar to a recent innovation in modelling biodiversity [40]. This will result in a more realistic framework for the log map, though an additional variance component needs to be incorporated into the normality proof and thus this is not a trivial extension of the procedure described here. This is an important limitation to note, and the author is continuing research in this direction.

7.3. Sources of tree-valued observations. Our examples in this paper have exclusively focused on using within-species variability to more accurately reflect variability in genetic data. However, many different processes give rise to phylogenetic tree-valued observations that could be used as inputs to this method. Gene trees, where each tree represents the phylogeny of a different location on the genome, provide another natural source of variability. However, there are two key considerations when using gene trees in

the above method. Firstly, it may not be a plausible assumption that gene trees would be observed from the same distribution, because “non tree–like” mechanisms may give rise to outlying gene trees. In these cases we advocate instead the procedures of [39], which was specifically invented as an outlier detection method, and [21, 20], which can be used to see the directions in which trees vary and gives a different perspective on outliers. Secondly, the above results rely on asymptotics: an evil necessitated because exact tree mean distributions are intractable in all nontrivial cases. It is most common to see 10 or fewer gene trees in phylogenetic studies, and it is unrealistic to think that asymptotic results provide utility with these sample sizes. Nevertheless, as sequencing continues to decrease in price, we can expect larger gene tree samples and the possibility of sufficiently large gene samples to use this method in the gene tree after outlier removal.

The method of [4], which was the first literature utilizing Fréchet means to find consensus trees, used Fréchet means and (scalar) Fréchet variance to analyze trees generated by Bayesian MCMC draws. Using our multivariate extension above, it is possible to consider multiple directions of variability in this context. Investigating the utility of multiple directions of variability to identify sources of model misspecification in the Bayesian context [27] is another promising area of future research.

7.4. Tree covariance. Having discussed the implications of violations to the assumption that observations are identically distributed in Section 7.3, we now discuss the assumption of independence. Ideally, tree–building information for n different individuals from each of the taxa on the tree would be obtained, and each individual from each taxa would be used only once to build n independent trees. However, when differing numbers of individuals are obtained from each taxa, a choice must be made between discarding information (to equalize the number individuals from each group) or inducing dependence by repeating some individuals when building the trees. In Section 6, we chose the latter option. This issue can be observed in Figures 2 and 3 via the clusters of the log mapped trees. Unfortunately, modeling this source of dependence and incorporating it into the covariance estimate $\hat{\Sigma}$ is extremely challenging, because it is likely that the extent of dependence between two trees $T_i, T_j \in \mathcal{T}_{m+3}$ depends not only on the number of shared individuals used to build the trees, but also on how closely related these individuals are on the tree (a function of the unknown true tree T^*). We conjecture that ignoring this dependence is a second–order issue compared to violations of identically and ignoring uncertainty in estimating the trees (Section 7.2). Investigation of this conjecture is an ongoing project of the

author.

8. Concluding remarks. The framework discussed here for representing collections of trees as points in Euclidean space opens phylogenetic tree analysis to many of the multivariate analysis methods that have been developed for Euclidean space. This paper considers only two such methods: confidence set construction for means, and a brief discussion on Euclidean PCA. However, testing two-sample hypotheses, discriminant analysis, multidimensional scaling and factor analysis could all be applied given an appropriate scientific question. However, it is important to note that in many cases key information about tree topologies that is relevant to an analysis will be lost when only the log map is considered. We are optimistic that the scientific community will exercise keen judgement in deciding whether to analyze and visualize trees in their native space or under the log map in the more interpretable Euclidean space.

This method advances recent innovations with respect to describing tree valued centre and variability, and can be considered a multivariate generalization of [20], though its flavor is more reminiscent of [4]. However, we believe the most important progress made in this manuscript is the application of the statistical framework of variance *modeling*, rather than minimizing, to tree space. Furthermore, the proposal for using species replicates to generate collections of trees for summary and analysis may prove fruitful by providing realistic measures of tree uncertainty. This is a known issue in phylogenetics and we hope that the sampling method and the confidence set construction procedure described here contributes to understanding of both of these issues.

Software. The trees and scripts used to generated Table 1, as well as R scripts for analysing the data in Section 6, are available from the author’s github page (User adw96). Requests for source code for the log map implementation should be emailed. R packages *ape*, *Rcmdr*, *scatterplot3d*, *rgl* and *mgcv* were used for the analysis and visualization, and we are grateful to the authors of these packages for their distribution.

Acknowledgements. The author is indebted to Professor Tom Nye of Newcastle University, who most kindly made available the code that underpins his PCA methods [20, 21], which assisted immensely in the implementation of the log map function. Additional thanks to John Bunge for suggestions that significantly clarified the exposition; Phil Spinks for encouragement and providing the turtle trees of Section 6.1; Giles Hooker and Marty Wells for funding that enabled completion of the project; and Sidney

Resnick and Louis Billera for their support of the investigation and helpful suggestions at a formative stage.

References.

- [1] BARDEN, D., LE, H. and OWEN, M. (2014). Limiting Behaviour of Fréchet Means in the Space of Phylogenetic Trees. *ArXiv:1409.7602*.
- [2] BAČÁK, M. (2014). Computing medians and means in Hadamard spaces. *SIAM Journal on Optimization* **24** 1542–1566.
- [3] BENNER, P. and BAČÁK, M. (2014). Computing the posterior expectation of phylogenetic trees. *ArXiv:1305.3692*.
- [4] BENNER, P., BAČÁK, M. and BOURGUIGNON, P.-Y. (2014). Point estimates in phylogenetic reconstructions. *Bioinformatics* **30** 534–540.
- [5] BHATTACHARYA, R. and LIN, L. (2016). Omnibus CLTs for Fréchet means and non-parametric inference on non-Euclidean spaces. *Proceedings of the American Mathematical Society*.
- [6] BILLERA, L. J., HOLMES, S. P. and VOGTMANN, K. (2001). Geometry of the space of phylogenetic trees. *Advances in Applied Mathematics* **27** 733–767.
- [7] CAVALLI-SFORZA, L. L. and EDWARDS, A. W. F. (1967). Phylogenetic Analysis Models and Estimation Procedures. *American Journal of Human Genetics* **19** 233–257.
- [8] FELSENSTEIN, J. (1983). Statistical Inference of Phylogenies. *Journal of the Royal Statistical Society: Series A* **146** 246–272.
- [9] GERARD, D., GIBBS, H. L. and KUBATKO, L. (2011). Estimating hybridization in the presence of coalescence using phylogenetic intraspecific sampling. *BMC evolutionary biology* **11** 291.
- [10] GUINDON, S. and GASCUEL, O. (2003). A Simple, Fast, and Accurate Algorithm to Estimate Large Phylogenies by Maximum Likelihood. *Systematic Biology* **52** 696–704.
- [11] HELED, J. and DRUMMOND, A. J. (2010). Bayesian inference of species trees from multilocus data. *Molecular Biology and Evolution* **27** 570–580.
- [12] HILLIS, D. M. and HUELSENBECK, J. P. (1994). Support for dental HIV transmission. *Nature* **369** 24–25.
- [13] HOTZ, T., HUCKEMANN, S., LE, H., MARRON, J. S., MATTINGLY, J. C., MILLER, E., NOLEN, J., OWEN, M., PATRANGENARU, V., SKWERER, S. and OTHERS (2013). Sticky central limit theorems on open books. *The Annals of Applied Probability* **23** 2238–2258.
- [14] JANKOVA, J. and VAN DE GEER, S. (2015). Confidence intervals for high-dimensional inverse covariance estimation. *Electronic Journal of Statistics* **9** 1205–1229.
- [15] LARKIN, M. A., BLACKSHIELDS, G., BROWN, N. P., CHENNA, R., McGEGGAN, P. A., McWILLIAM, H., VALENTIN, F., WALLACE, I. M., WILM, A., LOPEZ, R., THOMPSON, J. D., GIBSON, T. J. and HIGGINS, D. G. (2007). Clustal W and Clustal X version 2.0. *Bioinformatics* **23** 2947–2948.
- [16] LOGAN, I. S. (2016). ZIKA-How fast does this virus mutate? *Zoological Research* **37** 110.
- [17] MILLER, E., OWEN, M. and PROVAN, J. S. (2012). Averaging metric phylogenetic trees. *ArXiv:1211.7046*.
- [18] BBC MUNDO (2016). Zika: el bosque de Uganda de donde salió el virus que afecta a América Latina . www.bbc.com.
- [19] NORTIMÉRICA (2016). ¿De dónde procede el virus Zika? . www.notimerica.com.

- [20] NYE, T. M. (2011). Principal components analysis in the space of phylogenetic trees. *The Annals of Statistics* **39** 2716–2739.
- [21] NYE, T. M. W. (2014). An Algorithm for Constructing Principal Geodesics in Phylogenetic Treespace. *IEEE/ACM Transactions on Computational Biology and Bioinformatics* **11** 304–315.
- [22] OU, C.-Y., CIESIELSKI, C. A., MYERS, G. and OTHERS (1992). Molecular epidemiology of HIV transmission in a dental practice. *Science* **256** 1165–1171.
- [23] OWEN, M. and PROVAN, J. S. (2011). A fast algorithm for computing geodesic distances in tree space. *IEEE/ACM Transactions on Computational Biology and Bioinformatics* **8** 2–13.
- [24] RAMBAUT, A. and GRASS, N. C. (1997). Seq-Gen: an application for the Monte Carlo simulation of DNA sequence evolution along phylogenetic trees. *Computer applications in the biosciences* **13** 235–238.
- [25] RASMUSSEN, M. D. and KELLIS, M. (2012). Unified modeling of gene duplication, loss, and coalescence using a locus tree. *Genome Research* **22** 755–765.
- [26] REDNER, R. (1981). Note on the consistency of the maximum likelihood estimate for nonidentifiable distributions. *The Annals of Statistics* **9** 225–228.
- [27] REID, N. M., HIRD, S. M., BROWN, J. M., PELLETIER, T. A., MCVAY, J. D., SATLER, J. D. and CARSTENS, B. C. (2013). Poor fit to the multispecies coalescent is widely detectable in empirical data. *Systematic Biology*.
- [28] RENCHER, A. C. and CHRISTENSEN, W. F. (2012). Tests on Covariance Matrices. In *Methods of Multivariate Analysis*.
- [29] RONQUIST, F., TESLENKO, M., VAN DER MARK, P., AYRES, D. L., DARLING, A., HÖHNA, S., LARGET, B., LIU, L., SUCHARD, M. A. and HUELSENBECK, J. P. (2012). MrBayes 3.2: Efficient Bayesian phylogenetic inference and model choice across a large model space. *Systematic Biology* **61** 539–542.
- [30] ROYCHOUDHURY, A., WILLIS, A. and BUNGE, J. (2015). Consistency of a phylogenetic tree maximum likelihood estimator. *Journal of Statistical Planning and Inference* **161** 73–80.
- [31] SCADUTO, D. I., BROWN, J. M., HAALAND, W. C., ZWICKL, D. J., HILLIS, D. M. and METZKER, M. L. (2010). Source identification in two criminal cases using phylogenetic analysis of HIV-1 DNA sequences. *Proceedings of the National Academy of Sciences* **107** 21242–21247.
- [32] SHEN, S., SHI, J., WANG, J., TANG, S., WANG, H., HU, Z. and DENG, F. (2016). Phylogenetic analysis revealed the central roles of two African countries in the evolution and worldwide spread of Zika virus. *Virologica Sinica* **31** 118–130.
- [33] SPINKS, P. Q., THOMSON, R. C., PAULY, G. B., NEWMAN, C. E., MOUNT, G. and SHAFFER, H. B. (2013). Misleading phylogenetic inferences based on single-exemplar sampling in the turtle genus *Pseudemys*. *Molecular Phylogenetics and Evolution* **68** 269–281.
- [34] TIMM, N. H. (2002). Multivariate Distributions and the Linear Model. In *Applied Multivariate Analysis* 79–184. Springer.
- [35] WALD, A. (1949). Note on the consistency of the maximum likelihood estimate. *The Annals of Mathematical Statistics* 595–601.
- [36] WANG, L., VALDERRAMOS, S. G., WU, A., OUYANG, S. and OTHERS (2016). From mosquitos to humans: genetic evolution of Zika virus. *Cell host & microbe* **19** 561–565.
- [37] WEAVER, S. C., COSTA, F., GARCIA-BLANCO, M. A., KO, A. I., RIBEIRO, G. S., SAADE, G., SHI, P.-Y. and VASILAKIS, N. (2016). Zika virus: history, emergence, biology, and prospects for control. *Antiviral research* **130** 69–80.

- [38] WEYENBERG, G. (2016). Statistics in the Billera-Holmes-Vogtmann treespace.
- [39] WEYENBERG, G., HUGGINS, P. M., SCHARDL, C. L., HOWE, D. K. and YOSHIDA, R. (2014). KDETREES: non-parametric estimation of phylogenetic tree distributions. *Bioinformatics* **30** 2280–2287.
- [40] WILLIS, A., BUNGE, J. and WHITMAN, T. (2016). Improved detection of changes in species richness in high-diversity microbial communities. *ArXiv:1605.02082*.
- [41] ZIEZOLD, H. On expected figures and a strong law of large numbers for random elements in quasi-metric spaces. In *Transactions of the Seventh Prague Conference on Information Theory, Statistical Decision Functions, Random Processes and of the European Meeting of Statisticians* 591–602. Springer.

DEPARTMENT OF STATISTICAL SCIENCE
CORNELL UNIVERSITY
301 MALOTT HALL
ITHACA NY USA
adw96@cornell.edu